Blind calibration for arrays with an aberration layer in ultrasound imaging

Meulen, P. van der; Coutino, M.; Kruizinga, P.; Bosch, J.G.; Leus, G.

DOI
10.23919/Eusipco47968.2020.9287755

Publication date
2020

Document Version
Final published version

Published in
28th European Signal Processing Conference, EUSIPCO 2020 - Proceedings

Blind calibration for arrays with an aberration layer in ultrasound imaging

Pim van der Meulen*, Mario Coutino*, Pieter Kruizinga†, Johannes G. Bosch‡, Geert Leus*
*Delft University of Technology, Circuits and Systems, Delft, Netherlands
†Erasmus Medical Center, Department of Neuroscience, Rotterdam, Netherlands
‡Erasmus Medical Center, Department of Biomedical Engineering, Rotterdam, Netherlands

***Abstract*—We consider the scenario of finding the transfer function of an aberrating layer in front of an ultrasound array. We are interested in blindly estimating this transfer function without prior knowledge of the unknown ultrasound sources or ultrasound contrast image. The algorithm gives an exact solution if the matrix representing the aberration layer's transfer function is full rank, up to a scaling and reordering of its columns, which has to be resolved using some prior knowledge of the matrix structure. We provide conditions for the robustness of blind calibration in noise. Numerical simulations show that the method becomes more robust for shorter wavelengths, as the transfer function matrices then tend to be less ill-conditioned. Image reconstruction from simulated data using the k-Wave toolbox show that a well calibrated model removes some of the distortions introduced by an uncalibrated model, and improves the resolution for some of the sources.**

I. Introduction

In this contribution we consider the scenario of an aberrating layer in front of an ultrasound (US) array, as depicted in Fig. 1. In medical ultrasound imaging, such layers could represent the skin and fat layers to which the ultrasound probe is pressed to image internal organs. Furthermore, there is typically a small layer to match the impedance of the US probe and human skin, which causes some phase changes across the array. Another example is the human skull, which distorts ultrasound waves too strongly to use the resulting pulse-echo data to reconstruct an image of the brain with current imaging techniques. Recently, we have also investigated the use of so called 'coding masks', thin random phase masks, to reconstruct ultrasound images with a single US element. To successfully image using a coding mask, precise calibration is required but the current method measures the response of each pixel individually, which is time consuming. In all these cases, we are interested in estimating the effect of the aforementioned layers to incorporate it into the image reconstruction process.

A straightforward way of solving this problem would be to place sources or reflectors in known positions of the probe's field of view (FOV), and then adjust our model so as to match the expected response for that particular source to the measured response. Needless to say, this approach becomes problematic when we desire to adjust our ultrasound model for the human skull or the skin, since this would require us to place a multitude of sources inside the patient's skull or body. Moreover, such methods may be prone to positioning errors of such sources as well. Ideally, then, we would use a 'blind' calibration procedure that relies on some other principle to correct layer aberrations.

This work is part of the ASPIRE project (project 14926 within the STW OTP programme), which is financed by the Netherlands Organisation for Scientific Research (NWO).

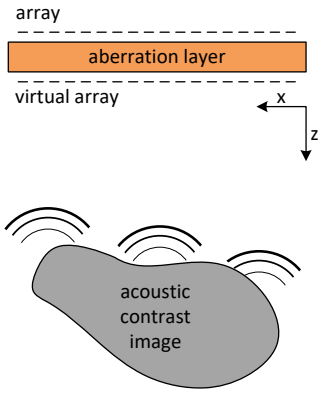

Fig. 1: An aberration layer distorts incident wavefields, leading to incorrect estimation of the acoustic contrast image. We are interested in estimating the transfer function from the virtual array just before the aberration layer to the real array.

In this paper, we generalize all problems above using the model as visualized in Fig. 1. We define a 'virtual' array, just in front of the aberration layer, and assume there is a linear transfer function from each point on the virtual array to each other point on the real array. The US field in the real array is then a linear combination of the field incident on the virtual array. We furthermore assume that the remainder of the FOV is a homogeneous medium, with only small inhomogeneities in the medium formed by the US contrast image that we want to reconstruct.

The problem of correcting for phase changes due to a phase screen in front of an US array has been studied before, using both blind and non-blind techniques. However, most of the studies focus on thin phase layers which cause a time delay for each point on the array (e.g., [1]–[3]). These methods only consider a time shift caused per element of the array, but do not consider situations where each sensor in the array may be influenced by multiple points on the virtual array.

Focusing ultrasound waves through the skull has been achieved using time-reversal techniques [4], and spatiotemporal filter design [5]. Unfortunately, these methods typically require one to first measure waves *inside* the brain. An interesting alternative approach is one where two arrays are placed opposite to one another on each side of the skull [6], avoiding the need for measurements inside the skull, but requiring two arrays. Furthermore, in [6] it is assumed that one of the skull walls can be approximated as a thin phase layer, which is not necessarily the case.

1) Notation: We will represent a vector $\mathbf{x}$ in lower-case bold, and a matrix $\mathbf{X}$ in upper-case bold. The operator $\|.\|_F$ represents the Frobenius norm, $\star$ represents the Khatri-Rao product, and $*$ denotes a temporal convolution. The notation $\mathbf{X}^\dagger$ represents the Moore-Penrose pseudo-inverse of $\mathbf{X}$. Finally, diag($\mathbf{c}$) stands for a diagonal matrix with the vector $\mathbf{c}$ on its diagonal.

II. Signal model and problem formulation

We assume that a linear array is placed in a homogeneous medium with linear propagation of US waves. We can either consider the case of a set of sources transmitting towards the array, or that a separate transmitter illuminates the FOV, where inhomogeneities (acoustic contrast) in the acoustic properties of the propagation medium scatter echoes towards the array. In the latter case, each contrast then acts as an independent source. If the contrasts are sufficiently weak, higher order reflections between reflectors can be ignored according to the Born approximation (see e.g. [7], [8]), which is typically used in ultrasound imaging. In that case, all measurements are linear w.r.t. sources and/or ultrasound contrast images, and we can use the following convolutional formulation to model measurements [9]–[11]. Denote the number of array elements by M, and the measurement of element m by $y_m(t)$. We divide the FOV in N small pixels, and assume that each from K sources transmits a signal $s_k(t)$. Our model then becomes:

$$y_m(t) = \sum_{n=1}^{N} x_n \; g^{(r)}_{m,n}(t) * \left(\sum_{k=1}^{K} g^{(t)}_{n,k}(t) * s_k(t) \right), \quad (1)$$

where $g^{(r)}_{m,n}(t)$ is the Green's function for a wave travelling from pixel n towards array element m, and x_n is the scatter intensity coefficient of pixel n. The signal $g^{(t)}_{n,k}(t)$ is the Green's function from source k to pixel n. Here, the superscript $^{(r)}$ refers to the receive Green's function (from a pixel to an array element), and the superscript $^{(t)}$ refers to the transmit Green's function.

Typically, the transfer functions and excitation signals are known beforehand, and the goal then is to estimate x_n from y_m. Since the y_m's are completely linear w.r.t. the x_n's, we can stack the measurements of all sensors for a single temporal frequency bin l into a single vector $\mathbf{y}_l \in \mathbb{C}^M$, and write:

$$\mathbf{y}_l = \mathbf{A}_l \mathbf{x}, \quad (2)$$

where $\mathbf{x} \in \mathbb{R}^N$ contains the coefficients x_n, and $\mathbf{A}_l \in \mathbb{C}^{M \times N}$ can be constructed using (1). This equation is typically used for solving the inverse imaging problem, i.e., finding the contrast image $\mathbf{x}$ from measurements $\mathbf{y}_l$, and is the equation we will try to solve for obtaining an image in the results section.

For the results in this paper we will mostly focus on calibration from many different transmit signals $s_k(t)$, using the equation below. From (1), we can express measurements as a linear function of the sources:

$$\begin{aligned} \mathbf{y}_l &= \mathbf{G}^{(r)}_l \text{diag}(\mathbf{x}) \mathbf{G}^{(t)}_l \mathbf{s}_l \\ &= \mathbf{G}_l \mathbf{s}_l, \end{aligned} \quad (3)$$

where $\mathbf{G}_l \triangleq \mathbf{G}^{(r)}_l \text{diag}(\mathbf{x}) \mathbf{G}^{(t)}_l$ has dimensions $M \times K$, and $\mathbf{s}_l \in \mathbb{C}^K$. If, instead of contrast sources scattering towards the array, there are K sources directly transmitting towards the array themselves, we set $\mathbf{G}^{(t)}_l = \mathbf{I}$, and $\mathbf{x}$ will be an all-zero vector with ones for the pixels where a transmitting source is active. *The latter will be the case for the simulations in this paper.* For the remainder of this paper, we drop the frequency subscript l, and we assume calibration is done on each frequency bin separately.

In the case of the presence of an aberration layer, there is an additional transfer function in the frequency domain from the ultrasound field just before the aberration layer to the ultrasound field in the positions of the array. That is, we introduce a virtual array just before the aberration layer, and assume there is a linear transfer function from each virtual array element to each element on the real array (Fig. 1). Hence, we can express the measurements $\mathbf{y}$ as

$$\mathbf{y} = \mathbf{H}\mathbf{G}\mathbf{s}, \quad (4)$$

where $\mathbf{H} \in \mathbb{C}^{M \times M}$ describes the linear mapping from US fields in the virtual array to the real array, for a single temporal frequency. Different from the original inverse imaging problem, the problem addressed in this paper is that of estimating $\mathbf{H}$ using equation (4) without knowledge of either $\mathbf{s}$ or $\mathbf{x}$.

III. Calibration algorithm

We start by trying to estimate $\mathbf{H}$ based on (4). Assume that P transmit events are used, using a K-element transmit array. We can stack the transmitted signals $\{\mathbf{s}(p) \in \mathbb{C}^K\}, p = 1, \ldots, P$ in a transmit matrix $\mathbf{S} = [\mathbf{s}(1)\ \mathbf{s}(2)\ \ldots\ \mathbf{s}(P)]$, and denote our first set of measurements as

$$\mathbf{Y}_1 = \mathbf{H}\mathbf{G}\mathbf{S}, \quad (5)$$

where $\mathbf{Y}_1 \in \mathbb{C}^{M \times P}$.

Next, we assume that a second set of measurements $\mathbf{Y}_2$ is obtained in a similar way, using the same image $\mathbf{x}$, and the same transmit sequences $\mathbf{S}$, but with a thin phase layer just in front of the virtual array. The thin phase layer causes a phase shift in the frequency domain on each point of the virtual array, so its effect can be modeled as:

$$\mathbf{Y}_2 = \mathbf{H}\mathbf{\Theta}\mathbf{G}\mathbf{S}, \quad (6)$$

where $\boldsymbol{\Theta} = \text{diag}(\boldsymbol{\theta})$, with $\boldsymbol{\theta} \in \mathbb{C}^M$ being the phase shifts of the thin phase layer. Such layers can be implemented using 'kinoforms' [12], [13], i.e., thin layers with a different speed of sound which cause a different time delay for each point on its surface by spatially varying the layer's thickness.

The basic idea of the calibration algorithm is to combine $\mathbf{Y}_1$ and $\mathbf{Y}_2$ as follows. First, $\mathbf{Y}_2$ is projected onto $\mathbf{Y}_1$:

$$\begin{aligned}\mathbf{Z} &= \mathbf{Y}_2\mathbf{Y}_1^\dagger \\ &= \mathbf{H}\boldsymbol{\Theta}\mathbf{G}\mathbf{S}(\mathbf{G}\mathbf{S})^\dagger\mathbf{H}^{-1} \\ &= \mathbf{H}\boldsymbol{\Theta}\mathbf{H}^{-1}. \end{aligned} \tag{7}$$

for which we require that $\mathbf{H}$ is invertible, and that $\mathbf{GS}$ is full row-rank, so that $\mathbf{GS}(\mathbf{GS})^\dagger = \mathbf{I}$.

This way, we obtain the matrix $\mathbf{Z}$ *which no longer depends on* $\mathbf{x}$ *or* $\mathbf{s}$. Moreover, the matrix $\mathbf{Z}$ has an eigendecomposition with eigenvectors $\mathbf{H}$ and eigenvalues $\boldsymbol{\theta}$. The aberration matrix can now be found using an eigendecomposition, without any prior knowledge of $\boldsymbol{\theta}$, provided that the eigendecomposition is unique. This can be ensured through the design of the thin phase layer, by making each delay in $\boldsymbol{\theta}$ unique. Through these steps, we have obtained the matrix $\mathbf{H}$ without *any prior knowledge* of the transmit codes $\mathbf{s}$ or the matrix $\mathbf{G}$. Note that this technique would also have worked with many contrast images, using $\mathbf{y} = \mathbf{HAx}$ from (2). In that case, $\mathbf{GS}$ in (7) would be replaced by $\mathbf{AX}$ and we would obtain $\mathbf{Z}$ as long as $\mathbf{AX}$ is full row-rank.

For the algorithm to be robust to noise, it is required that the matrix $\mathbf{Y}_1$ is well-conditioned, which in turn depends on $\mathbf{H}$, $\mathbf{G}$ and $\mathbf{S}$ to be well-conditioned (and full-rank). If $\mathbf{Y}_1$ is ill-conditioned, even small amounts of noise in $\mathbf{Y}_2$ can be amplified by the small singular values of $\mathbf{Y}_1$, resulting in a bad estimate of $\mathbf{Z}$.

This technique exploits a similar data structure as the one used in the well known ESPRIT algorithm [14]. Both ESPRIT and our method assume that two measurements are available, which are related by a diagonal matrix. In contrast to the ESPRIT algorithm, however, we are not interested in estimating the values on the diagonal of $\boldsymbol{\Theta}$, but in the eigenvector matrix $\mathbf{H}$. From a different point of view, (7) is the solution for $\mathbf{Z}$ for solving the equation $\mathbf{ZY}_1 = \mathbf{Y}_2$. Thus, by computing the eigendecomposition of $\mathbf{Z}$, we are performing a dynamic mode decomposition [15] on the data $\mathbf{Y}_1$ and $\mathbf{Y}_2$ to obtain $\mathbf{H}$ and $\boldsymbol{\theta}$.

A. Uniqueness

Since eigendecompositions are unique up to a reordering and scaling of the columns of $\mathbf{H}$, the order and scaling of the columns of the eigenvectors obtained from (7) are also ambiguous. To find the correct ordering, we assume that $\boldsymbol{\theta}$ is ordered in a known manner. For example, if $\theta_m = \exp(i2\pi m/M),\ m = 1, \ldots, M$, we may have the prior knowledge that $\{\theta_m\}$ are ordered by a linearly increasing phase component.

The scaling of each eigenvector of $\mathbf{Z}$ can be resolved according to various principles, but is very dependent on the aberration layer being studied. For example, a class of similar layers could be studied by simulations to find a parameterized common basis for the corresponding class of matrices. In the results section of this contribution, we focus on random aberration layers. We empirically found that the transfer function matrices of such layers have a strong Toeplitz structure per frequency (see Fig. 2 for a typical matrix of this class). Based on this prior knowledge, we will resolve the scaling issue by first defining a basis for the set of matrices a constant diagonal and constant subdiagonals, $\mathbf{B}_l \in \mathbb{C}^{M\times M},\ l = 1, \ldots,\ 2M-1$. We then try to minimize the Frobenius norm between this set of matrices and the (column-wise) scaled eigenvector matrix $\mathbf{H}_0$ of $\mathbf{Z}$, where $\mathbf{H}_0$ already has its columns re-ordered:

$$\{\hat{\mathbf{b}}, \hat{\mathbf{c}}\} = \arg\min_{\mathbf{b},\mathbf{c}\neq 0} \| \sum_{q=1}^{2M-1} b_q\mathbf{B}_q - \mathbf{H}_0\text{diag}(\mathbf{c})\|_F^2, \tag{8}$$

where $\mathbf{b} \in \mathbb{C}^{2M-1}$ contains the coefficients b_q, and $\mathbf{c} \in \mathbb{C}^M$ contains the scaling coefficients for each column of $\mathbf{H}_0$.

The solution of this problem, up to a complex scaling, is given by the smallest singular vector of the composite matrix $[\mathbf{B}\ (\mathbf{I} \star \mathbf{H})]$, with $\mathbf{B} = [\text{vec}(\mathbf{B}_1), \ldots \text{vec}(\mathbf{B}_{2M-1})]$. The resulting matrix $\hat{\mathbf{H}} = \mathbf{H}_0\text{diag}(\hat{\mathbf{c}})$ gives us an estimate of $\mathbf{H}$ up to a complex scaling of the entire matrix. Consequently, there is one final ambiguity, which is especially important when one wants to estimate an ultrasound image using all temporal frequencies jointly. The study of this problem is beyond the scope of this contribution, but solutions are available in literature. See e.g. [16] for tackling this problem structure, or [17]–[19] for solving this problem from covariance data.

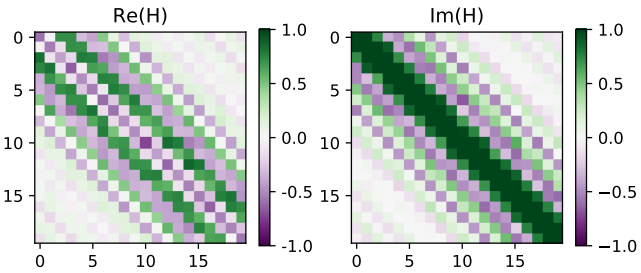

Fig. 2: An example of a typical $\mathbf{H}$ matrix of the random aberration layer in Fig. 3 for a temporal frequency of 5 MHz.

IV. Simulation results

To avoid the robustness issues described in the previous section, the calibration experiments have to be arranged and designed in such a way that $\mathbf{Y}_1$ and $\mathbf{Y}_2$ are well-conditioned and full rank matrices. To that end, we will assume the following experimental setup.

First, for simplicity, we will assume that a set of point sources are excited by some signals $\mathbf{S}$, which the sources transmit to the array. We will further place these sources in the far field, evenly distributed across directions of arrival from 0 to 180 degrees w.r.t. the array, causing the incident waves to be nearly plane when arriving at the aberration layer,

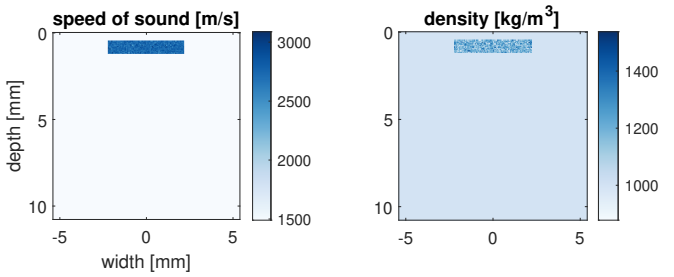

Fig. 3: Speed of sound and density distribution of the aberration layer used for the simulations in this contribution.

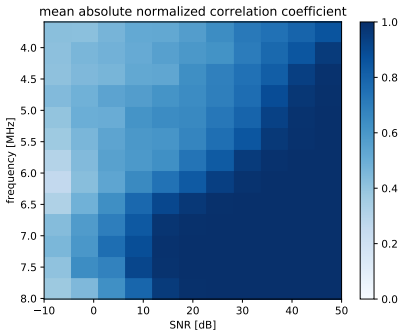

Fig. 4: Absolute correlation between the estimated transfer function matrix $\hat{\mathbf{H}}$ and the true $\mathbf{H}$ for various temporal frequencies and SNR values.

making $\mathbf{G}$ well-conditioned if all directions-of-arrival (DOAs) are covered. Note that $\mathbf{G}$ can also be well conditioned by taking a sufficiently large FOV in the imaging domain. We adopt the far-field in our simulation for simplicity for now. Second, we will use a random aberration layer as visualized in Fig. 3, which we empirically found to preserve information (i.e., $\mathbf{H}$ is a well-conditioned full rank matrix) relatively well. Finally, we use a white Gaussian matrix $\mathbf{S}$, so that $\mathbf{S}$ is full rank with high probability, and fully samples the column space of both $\mathbf{HG}$ and $\mathbf{H\Theta G}$. As a thin phase layer we choose one that causes a different phase shift for each point on the virtual array:

$$\theta_m = \exp(2\pi i(m - M/2)/M),\ m = 1, \ldots, M. \quad (9)$$

We obtain the true transfer function of the random layer by sampling $\mathbf{H}$ column-wise using the k-Wave ultrasound simulation toolbox [20]. The background medium in the simulations has the acoustic properties of water. We then generate $\mathbf{Y}_1$ and $\mathbf{Y}_2$ according to (5), (6), and (9), having obtained the $\mathbf{H}$ matrix as just described. In k-Wave, the medium is defined on a grid with a spacing of 50 μm, and we used an array of point sensors with a spacing of 200 μm, with $M = 20$. Signals are sampled in the time-domain using a sampling frequency of 206 MHz. For actual imaging simulations, in the next subsection, we focus on the frequency range of approximately 3-8 MHz.

A. General performance

First, we assess the performance of the algorithm for a range of noise levels. We define SNR with respect to $\mathbf{Y}_1$:

$$\text{SNR} = \frac{\|\mathbf{Y}_1\|_F^2}{\sigma_n^2 KM}, \quad (10)$$

where σ_n^2 is the noise variance, which we assume to be spatially and temporally white Gaussian i.i.d. noise. For the entries of $\mathbf{S}$ we use a realization of an i.i.d. Gaussian distribution, with $P = 1,000$. To find the correct order of the columns of $\mathbf{H}$, we sort the eigenvalues of $\mathbf{Z}$ according to their phase, and apply the same permutation to the columns of $\mathbf{H}$. To resolve the per-column scaling ambiguity, we solve (8) as described earlier. For each frequency and SNR, we compute a noisy $\mathbf{Y}_1$ and $\mathbf{Y}_2$ 100 times, and each time we compute the normalized correlation coefficient between $\mathbf{H}$ and $\hat{\mathbf{H}}$, defined as $\rho = \text{vec}(\mathbf{H})^{\mathsf{H}}\text{vec}(\hat{\mathbf{H}})/(\|\mathbf{H}\|_F\|\hat{\mathbf{H}}\|_F)$. As a final measure of performance, we show the mean absolute correlation over all 100 simulations.

The resulting performance is visualized in Fig. 4 for a range of SNRs and various frequencies. Performance increases with an increasing SNR, but also with increasing frequency. For higher frequencies, the size of inhomogeneities becomes closer to the wavelength, causing more scattering within the aberration layer, hence causing a more diverse transfer function matrix $\mathbf{H}$. For lower frequencies, the opposite happens: inhomogeneities are relatively small compared to the wavelength, and the layer mostly acts as a homogeneous layer. Such layers typically have a low-pass behaviour, i.e., the wavefield is smoothed out during propagation through the layer, reducing higher frequency content in the original wavefield. Consequently, the corresponding $\mathbf{H}$ matrix tends to be rank deficient or ill-conditioned, making it more difficult to estimate it from noisy measurements using the proposed method.

B. Imaging experiment

Next, we demonstrate the difference in terms of image reconstruction of a model calibrated using the proposed method, and an uncalibrated model. The parameter and simulation settings remain unchanged. For calibration, we use $P = 1,000$, using an SNR of 30 dB, but for the image reconstruction itself we only use one transmit event from the sources to the array. Furthermore, no noise is added to the array measurements used for image reconstruction since errors in the image are typically dominated by side and grating lobes. Note that in the calibration experiment we used far-field sources as described above, whereas in this simulation we consider sources positioned between the near and far field. All the sources inject a Gaussian pulse centered at 5 MHz, with a -6 dB bandwidth of approximately 4.5 MHz into the medium.

To obtain an image, we use the LSQR algorithm [21] to solve (2), using the result after 6 iterations to obtain a regularized estimate. For the uncalibrated model, we use $\mathbf{H} = \mathbf{I}$ to solve (2). The resulting image reconstructions are shown in Fig. 5 and 6. As can be seen, the layer mostly distorts by spatially shifting and stretching the true image, which is resolved by using the calibrated model. Moreover, without

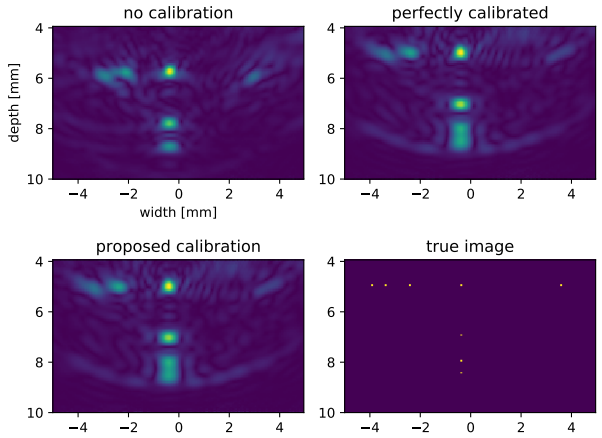

Fig. 5: Image reconstructions of a resolution phantom in k-Wave. We compare reconstruction with no calibration, a perfectly calibrated model, and a calibrated model using the proposed method.

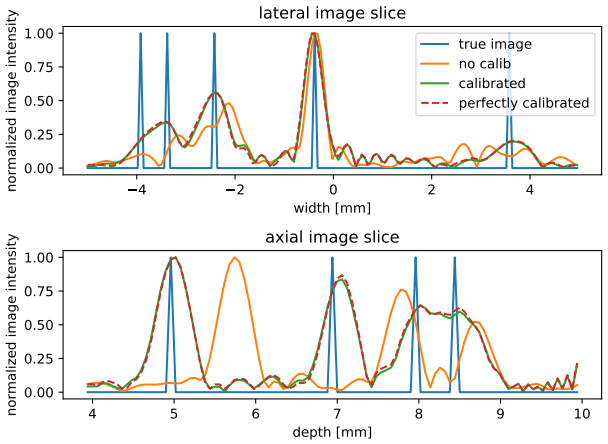

Fig. 6: Lateral and axial profiles of the reconstructions of Fig. 5.

calibration some of the sources are not visible, such as the fourth source in the axial slice of the image in Fig. 6, and the rightmost source in the lateral slice.

V. Conclusion

In this contribution we considered the problem of estimating the transfer function matrix of an aberrating layer in front of an (ultrasound) array. The proposed method does not require knowledge of the ultrasound image/sources, but is dependent on the proper conditioning of the blind calibration problem. Consequently, blind calibration becomes more robust to additive noise for higher temporal frequencies, where the transfer function matrices become more well-conditioned. In noiseless scenarios, the algorithm gives an exact solution of the transfer function matrix, up to a scaling and permutation of its columns. This ambiguity is resolved in this paper by assuming that the transfer function matrix has a strong Toeplitz structure, which we empirically found to be the case for random aberration layers. Finally, we demonstrated that using a calibrated model for imaging reduces the geometric distortion introduced by a random aberration layer, and additionally is able to reveal sources that are hard to resolve for the uncalibrated model.

References

[1] L. Nock, G. E. Trahey, and S. W. Smith, "Phase aberration correction in medical ultrasound using speckle brightness as a quality factor," *The Journal of the Acoustical Society of America*, vol. 85, no. 5, pp. 1819–1833, 1989.

[2] M. Karaman, A. Atalar, H. Koymen, and M. O'Donnell, "A phase aberration correction method for ultrasound imaging," *IEEE transactions on ultrasonics, ferroelectrics, and frequency control*, vol. 40, no. 4, pp. 275–282, 1993.

[3] M. O'donnell and S. Flax, "Phase-aberration correction using signals from point reflectors and diffuse scatterers: Measurements," *IEEE transactions on ultrasonics, ferroelectrics, and frequency control*, vol. 35, no. 6, pp. 768–774, 1988.

[4] M. Fink, D. Cassereau, A. Derode, C. Prada, P. Roux, M. Tanter, J.-L. Thomas, and F. Wu, "Time-reversed acoustics," *Reports on progress in Physics*, vol. 63, no. 12, p. 1933, 2000.

[5] J.-F. Aubry, M. Tanter, J. Gerber, J.-L. Thomas, and M. Fink, "Optimal focusing by spatio-temporal inverse filter. ii. experiments. application to focusing through absorbing and reverberating media," *The Journal of the Acoustical Society of America*, vol. 110, no. 1, pp. 48–58, 2001.

[6] F. Vignon, J. Aubry, M. Tanter, A. Margoum, and M. Fink, "Adaptive focusing for transcranial ultrasound imaging using dual arrays," *The Journal of the Acoustical Society of America*, vol. 120, no. 5, pp. 2737–2745, 2006.

[7] J. T. Fokkema and P. M. van den Berg, *Seismic applications of acoustic reciprocity*. Elsevier, 1993.

[8] M. Verweij, B. Treeby, K. Van Dongen, and L. Demi, "Simulation of ultrasound fields," *Comprehensive biomedical physics*, pp. 465–499, 2014.

[9] P. R. Stepanishen, "Pulsed transmit/receive response of ultrasonic piezoelectric transducers," *The Journal of the Acoustical Society of America*, vol. 69, no. 6, pp. 1815–1827, 1981.

[10] J. A. Jensen, "A model for the propagation and scattering of ultrasound in tissue," *The Journal of the Acoustical Society of America*, vol. 89, no. 1, pp. 182–190, 1991.

[11] J. A. Jensen and N. B. Svendsen, "Calculation of pressure fields from arbitrarily shaped, apodized, and excited ultrasound transducers," *IEEE transactions on ultrasonics, ferroelectrics, and frequency control*, vol. 39, no. 2, pp. 262–267, 1992.

[12] K. Melde, A. G. Mark, T. Qiu, and P. Fischer, "Holograms for acoustics," *Nature*, vol. 537, no. 7621, pp. 518–522, 2016.

[13] M. Brown, D. Nikitichev, B. Treeby, and B. Cox, "Generating arbitrary ultrasound fields with tailored optoacoustic surface profiles," *Applied Physics Letters*, vol. 110, no. 9, p. 094102, 2017.

[14] R. Roy and T. Kailath, "Esprit-estimation of signal parameters via rotational invariance techniques," *IEEE Transactions on acoustics, speech, and signal 995*, 1989.

[15] P. J. Schmid, "Dynamic mode decomposition of numerical and experimental data," *Journal of fluid mechanics*, vol. 656, pp. 5–28, 2010.

[16] S. Ling and T. Strohmer, "Self-calibration and bilinear inverse problems via linear least squares," *SIAM Journal on Imaging Sciences*, vol. 11, no. 1, pp. 252–292, 2018.

[17] S. J. Wijnholds and A.-J. Van Der Veen, "Multisource self-calibration for sensor arrays," *IEEE Transactions on Signal Processing*, vol. 57, no. 9, pp. 3512–3522, 2009.

[18] P. van der Meulen, P. Kruizinga, J. G. Bosch, and G. Leus, "Calibration techniques for single-sensor ultrasound imaging with a coding mask," in *2018 52nd Asilomar Conference on Signals, Systems, and Computers*. IEEE, 2018, pp. 1641–1645.

[19] K. N. Ramamohan, S. P. Chepuri, D. F. Comesana, and G. Leus, "Blind calibration of sparse arrays for doa estimation with analog and one-bit measurements," in *ICASSP 2019-2019 IEEE International Conference on Acoustics, Speech and Signal Processing (ICASSP)*. IEEE, 2019, pp. 4185–4189.

[20] B. E. Treeby and B. T. Cox, "k-wave: Matlab toolbox for the simulation and reconstruction of photoacoustic wave fields," *Journal of biomedical optics*, vol. 15, no. 2, p. 021314, 2010.

[21] C. C. Paige and M. A. Saunders, "Lsqr: An algorithm for sparse linear equations and sparse least squares," *ACM Transactions on Mathematical Software (TOMS)*, vol. 8, no. 1, pp. 43–71, 1982.